Lawrence Berkeley National Laboratory
Joint Genome Institute

Title
Novel Monomeric Fungal Subtilisin Inhibitor from a Plant-Pathogenic Fungus, Choanephora cucurbitarum: Isolation and Molecular Characterization.

Permalink
https://escholarship.org/uc/item/0ps430rq

Journal
Applied and Environmental Microbiology, 86(22)

ISSN
0099-2240

Authors
Pathiraja, Duleepa
Chun, Youngeun
Cho, Junghwan
et al.

Publication Date
2020-10-28

DOI
10.1128/aem.01818-20

Peer reviewed

Novel Monomeric Fungal Subtilisin Inhibitor from a Plant-Pathogenic Fungus, *Choanephora cucurbitarum*: Isolation and Molecular Characterization

Duleepa Pathiraja,[a] Youngeun Chun,[a] Junghwan Cho,[a] Byoungnam Min,[a] Saeyoung Lee,[a] Hongjae Park,[a] Juan Byun,[a] In-Geol Choi[a]

[a]Department of Biotechnology, College of Life Sciences and Biotechnology, Korea University, Seoul, Republic of Korea

Duleepa Pathiraja and Youngeun Chun contributed equally to this work. Author order was determined by the contribution to analyzing data and writing the manuscript.

ABSTRACT The bacterial protease inhibitor domains known as *Streptomyces* subtilisin inhibitors (SSI) are rarely found in fungi. Genome analysis of a fungal pathogen, *Choanephora cucurbitarum* KUS-F28377, revealed 11 SSI-like domains that are horizontally transferred and sequentially diverged during evolution. We investigated the molecular function of fungal SSI-like domains of *C. cucurbitarum*, designated "choanepins." Among the proteins tested, only choanepin9 showed inhibitory activity against subtilisin as the target protease, accounting for 47% of the inhibitory activity of bacterial SSI. However, the binding affinity (expressed as the dissociation constant [K_d]) of choanepin9 measured via microscale thermophoresis was 21 nM, whereas that for bacterial SSI is 34 nM. The trend of binding and inhibitory activity suggests that the two inhibitors exhibit different inhibitory mechanisms for subtilisin protease. Interestingly, choanepin9 was identified as a monomer in studies *in vitro*, whereas bacterial SSI is a homodimer. Based on these observations, we constructed a monomeric bacterial SSI protein with decreased binding affinity to abrogate its inhibitory activity. By altering the reactive sites of choanepin9 deduced from the P1 and P4 sites of bacterial SSI, we reestablished that these residues in choanepins are also crucial for modulating inhibitory activity. These findings suggest that the fungal SSI evolved to target specific cognate proteases by altering the residues involved in inhibitory reactivity (reactive sites) and binding affinity (structural integrity). The function of fungal SSI proteins identified in this study provides not only a clue to fungal pathogenesis via protease inhibition but also a template for the design of novel serine protease inhibitors.

IMPORTANCE Until recently, *Streptomyces* subtilisin inhibitors (SSI) were reported and characterized only in bacteria. We found SSI-like domains in a plant-pathogenic fungus, *Choanephora cucurbitarum* KUS-F28377, which contains 11 sequentially diverged SSI-like domains. None of these fungal SSI-like domains were functionally characterized before. The active form of fungal SSI-like protein is a monomer, in contrast to the homodimeric bacterial SSI. We constructed a synthetic monomer of bacterial SSI to demonstrate the modulation of its activity based on structural integrity and not reactive sites. Our results suggest the duplication and divergence of SSI-like domains of *C. cucurbitarum* within the genome to inhibit various cognate proteases during evolution by modulating both binding and reactivity. The molecular functional characterization of fungal SSI-like domains will be useful in understanding their biological role and future biotechnological applications.

KEYWORDS *Streptomyces* subtilisin inhibitor, fungal protease inhibitor, *Choanephora cucurbitarum*

Proteinaceous protease inhibitors are distributed among a wide variety of living organisms, ranging from microorganisms to plants and animals (1–3). Primary targets of protease inhibitors include intra- and extracellular proteases, whose activity is precisely controlled in the cellular environment. The physiological role of protease inhibitors differs in different organisms. Protease inhibitors found in insects play key roles in digestion, reproduction, the complement system, and the innate immune response (4). Mammalian protease inhibitors are involved in tightly regulated physiological processes such as blood coagulation, host defense, inflammation, and ischemia protection (5). Most protease inhibitors in plants play an important role in host defense by inhibiting the proteases of pests and pathogens (6–8).

A bacterial protease inhibitor isolated from the genus *Streptomyces* is recognized as a strong inhibitor of a serine protease known as subtilisin. Thus, these inhibitors are classified as *Streptomyces* subtilisin inhibitors (SSI) (9). The first SSI was discovered in *Streptomyces albogriseolus* (10), and several other homologous inhibitors from the same genus have been characterized (11). According to the MEROPS database (https://www.ebi.ac.uk/merops/), SSI belong to the inhibitor family I16. The members of the I16 family inhibit their target serine endopeptidases, including subtilisin (12), kexin (13), trypsin, plasmin (14), and SAM-P20 (15). The inhibitory activity is often specific and depends on the type of cognate serine protease. Analysis of 3-dimensional structure revealed that the active form of SSI is a homodimer, and each subunit interacted noncovalently with the active site of the cognate protease in a 1:1 molar ratio (16). SSI has an extended flexible region that fits into the active site of subtilisin (17). In particular, the β-sheet interactions between SSI and subtilisin (the P1 to P6 residues of bacterial SSI and the S1 to S6 sites of subtilisin) play an important role in the rigidification of the enzyme-inhibitor complex (16). The amino acid residues in the P1 (Met73) and P4 (Met70) reactive sites have been regarded as the major determinants of the specificity of bacterial SSI (9, 18, 19). Two disulfide linkages near the reactive site maintain the stability of bacterial SSI (16).

Recent genome analysis of a plant-pathogenic fungus, *Choanephora cucurbitarum* KUS-F28377, revealed 11 putative genes containing SSI-like domains (20). *C. cucurbitarum* is a well-known plant pathogen, causing fruit and blossom rot in cucurbits and other plants (21). Proteases and protease inhibitors play dynamic roles in plant pathogenesis and host defense (22). In plants, subtilisin-like proteases are part of the pathogen recognition and host defense mechanism, while SSI may facilitate the evasion of host defense (23). Phylogenetic analysis suggested that these fungal SSI-like domains might be transferred horizontally, and their cellular function was predicted as producing virulence factors that enabled pathogenic fungi to bypass the host defense mechanism (20). Although the fungal SSI-like domains were predicted by sequence similarity, the functional characterization of fungal domains and the identification of their cognate proteases have yet to be reported.

Here, we report the molecular functionality of the novel fungal SSI-like inhibitory domains from a pathogenic fungus, *C. cucurbitarum* KUS-F28377, by examining their inhibitory activity against subtilisin. The molecular features of three putative fungal SSI-like domains were compared with those of the known bacterial SSI derived from *S. albogriseolus*. We mutated critical amino acid residues of fungal SSI-like proteins to modulate the inhibitory activity and measured the binding affinity of mutants via microscale thermophoresis (MST). These experiments demonstrated the functional roles of the reactivity (reactive P1 and P4 sites) and binding affinity (residues contributing to structural integrity) of fungal SSI-like proteins. Our results summarize the functional similarity and peculiarity of both bacterial and fungal SSI domains, providing a clue to the biological role of SSI domains and a guide for the design of novel serine protease inhibitors.

RESULTS

Sequential and structural analysis of SSI-like domains in *C. cucurbitarum*. Proteins possessing SSI-like domains are extremely rare within the fungal kingdom. We

identified 11 *C. cucurbitarum* proteins containing SSI-like domains and designated them choanepins based on the nomenclature of classical protease inhibitors. Further, we identified seven other fungal proteins containing SSI-like domains, including one in *Absidia repens*, three in *Absidia glauca*, and three in *Basidiobolus meristosporus*, by searching the Pfam database (as of December 2019). Additionally, six bacterial SSI protein sequences belonging to the genus *Streptomyces* were retrieved for comparative sequence analysis.

We constructed a multiple sequence alignment using all available fungal SSI-like proteins and six representative bacterial SSI proteins (Fig. 1a). The 3-dimensional structure of the SSI derived from *S. albogriseolus* (*Sal*SSI) (PDB ID 2SIC) was included in the alignment as the reference structure. The structural features of bacterial SSI suggest that *Sal*SSI (i) is functional in a homodimer (16), (ii) has a long flexible loop that fits into the substrate binding pockets of subtilisin protease (17), (iii) has two reactive P1 and P4 sites (Met73 and Met70, respectively, in the loop region modulate activity against specific target proteases) (9, 18, 19), and (iv) has two disulfide bonds and a major contact (Arg90) in the dimeric interface that contribute to structural integrity (19) (Fig. 1b). Four cysteine residues known to build a disulfide linkage are highly conserved in all SSI-like proteins except for one, choanepin8 (Fig. 1a). Although the P1 and P4 sites in the long loop region are critical for substrate recognition and activity in bacterial SSI domains (9, 18, 19), the amino acid residues in the loop region are variable and less conserved. Also, extended amino-terminal regions were observed in some fungal SSI-like proteins (*A. glauca* SSI1 [*Agl*SSI1], *Agl*SSI2, choanepin2, and choanepin6).

All 25 of these SSI-like proteins were used to build a gene tree based on the amino acid sequence (Fig. 1c). In the tree, the fungal SSI proteins were grouped according to the origin of the species, but the orthologous relationship was not obvious, implying that most genes duplicated and diverged within the genomes. All the fungi except *A. repens* carry multiple genes encoding SSI-like protein domains. We observed a similar pattern within the bacterial genus *Streptomyces*, which consists of bacteria mostly harboring duplicated SSI domains in their genomes (data not shown).

Examination of subtilisin inhibition by choanepins *in vitro*. For functional characterization, we arbitrarily selected three choanepins: choanepin3 (UniProt ID A0A1C7MXR2), choanepin8 (A0A1C7N6D3), and choanepin9 (A0A1C7N2Q4). Choanepin9 showed higher amino acid identity (36%) to *Sal*SSI than choanepin8 (33% identity) and choanepin3 (28% identity). Since the natural substrate of choanepins is still unknown, we selected subtilisin as the target protease owing to the high sequence similarity of choanepins to bacterial SSI-like proteins. Only choanepin9 showed inhibitory activity, whereas no or very low activity was detected with choanepin3 and choanepin8 when subtilisin was used as the target protease (Table 1). The inhibitory activity of choanepins was compared with those of the known proteinaceous and chemical subtilisin inhibitors, bacterial SSI from *S. albogriseolus* (*Sal*SSI) and phenylmethane sulfonyl fluoride (PMSF). To improve the solubility of choanepins, we designed additional constructs that were fused to maltose binding protein (MBP) (designated choanepin3M, choanepin8M, choanepin9M, and *Sal*SSIM below). Choanepin9M also inhibited subtilisin, and its specific inhibitory activity was equivalent to that of choanepin9 (Table 1). Like choanepins without MBP fusion, choanepin3M and choanepin8M did not show detectable inhibitory activity against subtilisin, and no adverse effects were associated with amino-terminal fusion to SSI domains.

To determine the substrate specificity of choanepin9, we used three additional proteinases: proteinase K, trypsin, and α-chymotrypsin. Choanepin9 did not show any inhibitory activity against these proteases (see Fig. S1 in the supplemental material). Although proteinase K is a serine protease, chaonepin9 did not show any inhibitory activity. In contrast, *Sal*SSI inhibited proteinase K but was inactive against trypsin and α-chymotrypsin, as reported in the literature (19).

The active oligomeric state of a bacterial SSI derived from *S. albogriseolus* (*Sal*SSI) is a homodimer, and each dimer binds to two subtilisin proteases (24). The optimal molar
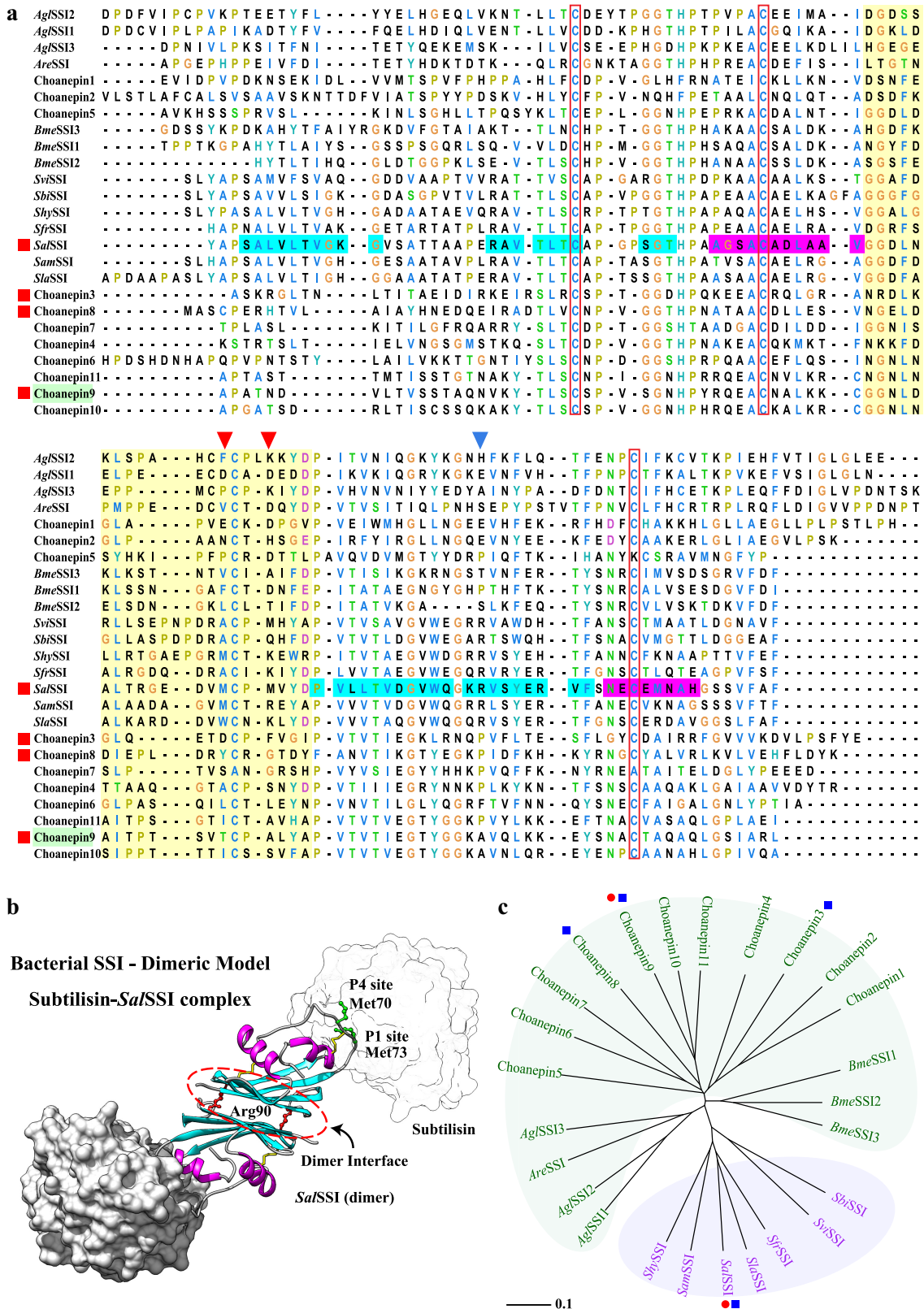
FIG 1 Sequential and structural analysis of the representative bacterial and fungal SSI-like domains. (a) Multiple sequence alignment of all 18 available fungal SSI-like proteins (11 from *C. cucurbitarum*, 3 from *A. glauca*, 1 from *A. repens*, and 3 from *B. meristosporus*) and 7 representative bacterial SSI proteins, including the *S. albogriseolus* SSI (*Sal*SSI), representing a reference structure (PDB ID 2SIC). Three choanepin sequences (choanepin3, choanepin8, and choanepin9) and a bacterial SSI (*Sal*SSI) studied in this work are labeled with red

TABLE 1 Inhibitory activities of fungal SSI-like proteins against subtilisin

Inhibitor	Residual activity of subtilisin (%)[a]	Specific inhibitory activity (U/mg)[a]
Choanepin8	98.6 ± 1.1	0.009 ± 0.002
Choanepin9	53.7 ± 1.9	0.471 ± 0.022
Choanepin3	ND[b]	ND
SalSSI	4.8 ± 0.4	0.534 ± 0.060
Choanepin8M	94.2 ± 1.1	0.012 ± 0.003
Choanepin9M	48.7 ± 2.1	0.305 ± 0.028
Choanepin3M	97.0 ± 2.9	0.010 ± 0.005
SalSSIM	3.4 ± 0.4	0.574 ± 0.030
PMSF	2.3 ± 1.4	NA[c]

[a]Data are presented as means ± standard deviations ($n = 3$).
[b]ND, not determined.
[c]NA, not applicable; specific activity was not determined for the chemical inhibitor.

ratio of bacterial SSI to subtilisin was determined as 1:1 (16, 24). We analyzed the optimal molar stoichiometry of choanepin9 by titrating with subtilisin. Increasing the molar ratio of choanepin9 to subtilisin gradually overcame the inhibitory activity of choanepin9 against subtilisin (Fig. 2a). When the molar ratio was 4:1 (choanepin9 to subtilisin), we observed complete inhibition (Fig. 2a). In contrast, SalSSI showed complete inhibition of subtilisin at a molar ratio of 1:1 (SalSSI to subtilisin), as reported previously (24) (Fig. 2b). This finding suggested that the mechanism of inhibition or binding pattern of choanepin differed from that of SalSSI.

Stability of the subtilisin-choanepin9 complex. The inhibitory activity of choanepin9 was decreased by different incubation times (30 min versus 60 min), suggesting that the subtilisin-choanepin9 complex was less stable than the subtilisin-SalSSI complex (Fig. 2a). To determine the stability of the enzyme-inhibitor complex, 1 U of subtilisin was incubated with choanepin9, and the residual subtilisin activity was determined at different time intervals (Fig. 3). Additionally, subtilisin was incubated with PMSF and bovine serum albumin (BSA) in order to compare chemical inhibition and the stability of subtilisin without a protease inhibitor. Minimal subtilisin activity was observed with PMSF, and subtilisin activity was maintained similarly to its initial activity when a protease inhibitor was not used. The half-life of the subtilisin-choanepin9 complex was 1 h at 37°C and pH 7.4. Within 12 h, the inhibitory activity of choanepin9 disappeared, and 90% of initial subtilisin activity was recovered, indicating the degradation of the subtilisin-choanepin9 complex. In contrast, the subtilisin-SalSSI complex showed much higher stability under similar conditions. The half-life of subtilisin-SalSSI was determined to be 34 h, which may be attributed to the highly specific binding of SalSSI to its cognate protease subtilisin.

Identifying the oligomeric state of active choanepin9. We determined experimentally, via native gel electrophoresis and size exclusion chromatography, that cho-

FIG 1 Legend (Continued)
squares. The reactive P1 and P4 amino acid residues are indicated by inverted red triangles. The disulfide cysteines are boxed in red in the alignment. The critical residue (Arg90) in the dimeric interface of bacterial SSI is indicated by an inverted blue triangle. Rectangular cyan and magenta boxes in the alignment of SalSSI indicate the β-sheet and α-helix structural elements, respectively. The less-conserved amino termini (including signal peptide regions) of all SSI were truncated to avoid spurious alignments. (b) Three-dimensional structure model of dimeric SalSSI (PDB ID 2SIC) bound to subtilisin. In a SalSSI-subtilisin complex, the key amino acid residues involved in reactivity and structural integrity are indicated by stick (disulfide bonds) and ball-and-stick (key residues: Met70, Met73, and Arg90) models. The reactive P1 and P4 sites (Met73 and Met70, respectively) are shown in green, and Arg90 in the dimeric interface is shown in red. (c) Gene tree of all 25 SSI-like proteins based on the amino acid sequences. The gene tree was constructed using the neighbor joining method with 100 bootstrap iterations. The proteins (with their UniProt accession numbers in parentheses) are as follows: *Absidia glauca* SSI1 (AglSSI1) (A0A168QS89), AglSSI2 (A0A168LVH5), AglSSI3 (A0A168QS75); *Absidia repens* SSI (AreSSI) (A0A1X2I8B2); *Basidiobolus meristosporus* SSI1 (BmeSSI1) (A0A1Y1ZBL2), BmeSSI2 (A0A1Y1Z6T9), BmeSSI3(A0A1Y1YKF4); choanepin1(A0A1C7NCP9), choanepin2 (A0A1C7N8R7), choanepin3 (A0A1C7MXR2), choanepin4 (A0A1C7NK99), choanepin5 (A0A1C7NNR9), choanepin6 (A0A1C7MZ12), choanepin7 (A0A1C7N1C9), choanepin8 (A0A1C7N6D3), choanepin9 (A0A1C7N2Q4), choanepin10 (A0A1C7NV11), and choanepin11 (A0A1C7NIW1) of *C. cucurbitarum*; *S. albogriseolus* SSI (SalSSI) (P01006); *Streptomyces virginiae* SSI (SviSSI) (P80388); *Streptomyces bikiniensis* SSI (SbiSSI) (Q9R645); *Streptomyces hygroscopicus* SSI (ShySSI) (Q9R641); *Streptomyces fradiae* SSI (SfrSSI) (Q9R643); *Streptomyces ambofaciens* SSI (SamSSI) (Q9R642); *Streptomyces lavendulae* SSI (SlaSSI) (P29609). Three choanepin sequences (choanepin3, choanepin8, and choanepin9) and a bacterial SSI (SalSSI) studied in this work are labeled with blue squares. Choanepin9 and SalSSI, which were used in mutational studies, are labeled with red circles.
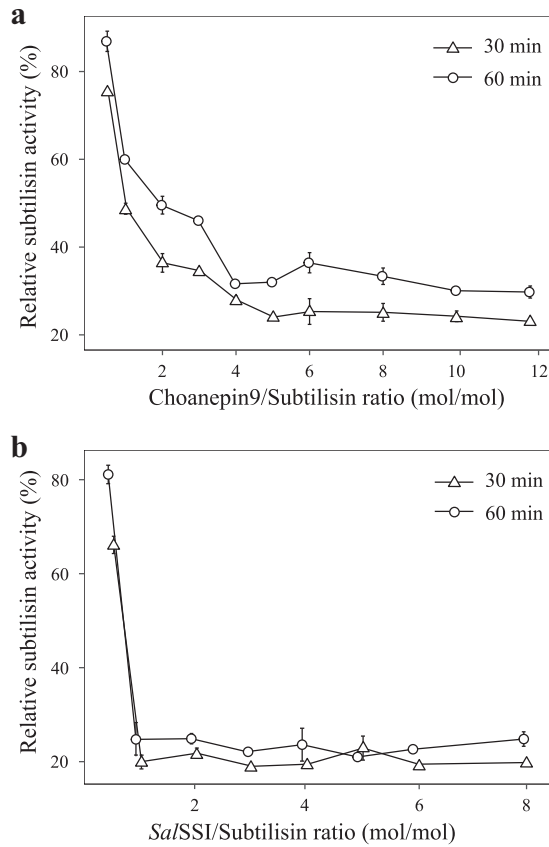
FIG 2 Stoichiometry of subtilisin inhibition. The stoichiometry of enzyme-inhibitor binding was determined by varying the molar ratio of choanepin9 or *Sal*SSI to subtilisin. Residual subtilisin activity was measured at different molar ratios between choanepin9 and subtilisin (a) or *Sal*SSI and subtilisin (b). Reactions were carried out for 30 min and 60 min separately at 37°C in a buffer containing 20 mM Tris-Cl, 100 mM NaCl (pH 7.5). Graphs were plotted using the residual subtilisin activity at different molar ratios. Data are presented as means $\pm$ standard deviations ($n = 3$).

anepin9 is a monomer in its active form. Based on the sizes and patterns predicted for the oligomerization of native and MBP-fused proteins, we analyzed equimolar combinatorial protein mixtures via native agarose gel electrophoresis (Fig. S2). The *Sal*SSI-*Sal*SSIM mixture showed different migration patterns of homogeneous mixtures (e.g., *Sal*SSI-*Sal*SSIM versus *Sal*SSI-*Sal*SSI or *Sal*SSIM-*Sal*SSIM). In contrast, the migration pattern of the choanepin9-choanepin9M mixture remained constant relative to that of the homogeneous mixtures of individual proteins.

Additional experimental evidence was derived from size exclusion chromatography. We again used both native (*Sal*SSI and choanepin9) and MBP-fused (*Sal*SSIM and choanepin9M) proteins in size exclusion chromatography. The theoretical molecular weights (MW) of *Sal*SSIM, *Sal*SSI, choanepin9M, and choanepin9 are 55.2 kDa, 11.5 kDa, 53.9 kDa, and 10.3 kDa, respectively. The major peaks of the high-performance liquid chromatography (HPLC) chromatogram represent dimers of *Sal*SSIM and *Sal*SSI and monomers of choanepin9M and choanepin9 (Fig. 4). Further, we tested the oligomeric states with equimolar mixtures of native and MBP-fused proteins. The *Sal*SSI-*Sal*SSIM mixture showed three chromatographic peaks corresponding to dimers of *Sal*SSIM-*Sal*SSIM (134.4 kDa; theoretical MW, 110.4 kDa), *Sal*SSI-*Sal*SSIM (58.0 kDa; theoretical MW, 66.7 kDa), and *Sal*SSI-*Sal*SSI (13.9 kDa; theoretical MW, 23.0 kDa) (Fig. 4b). However, the chromatogram of the choanepin9-choanepin9M mixture showed only two peaks, corresponding to choanepin9M (46.1 kDa) and choanepin9 (9.5 kDa) (Fig. 4c). These two peaks represent the monomeric forms of choanepin9 and choanepin9M without any cross-interactions.
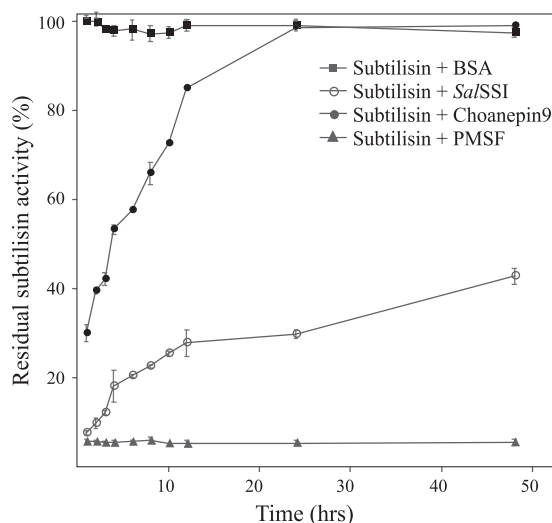
FIG 3 Stability of the subtilisin-inhibitor complex. The stabilities of the choanepin9-subtilisin and SalSSI-subtilisin complexes were determined by measuring residual subtilisin activity at different time intervals. Subtilisin was incubated with a saturating amount of choanepin9 or SalSSI separately at 37°C in a buffer containing 20 mM Tris-Cl, 100 mM NaCl (pH 7.5), and residual subtilisin activity was determined. PMSF and BSA were used to determine the effect of chemical inhibition over time and the stability of subtilisin without a protease inhibitor. Graphs were plotted using the residual subtilisin activity at different time intervals. Data are presented as means $\pm$ standard deviations ($n = 3$).

Measuring the binding affinity of choanepin9M via MST. The affinities of choanepin9M and SalSSIM for subtilisin were determined via microscale thermophoresis (MST) in order to ascertain whether the observed activity correlated with binding affinity. We labeled choanepin8M, choanepin9M, SalSSIM, and MBP (negative control) to titrate subtilisin and determine the binding affinity of choanepin (or SalSSI) for subtilisin (Fig. 5; Table 2). The dissociation constants (K_d) of choanepin9M and SalSSIM were calculated as 21 nM and 34 nM, respectively, at 25°C. However, the data points obtained for choanepin8M and MBP did not fit the dose-response curves of the specific binding interactions (Fig. 5a).

Mutational analysis of key amino acid residues related to reactivity and structural integrity. We analyzed the roles of key amino acid residues related to the reactivity and structural integrity of choanepin9 via site-directed mutagenesis. Mutational studies indicated that it was mainly the altered reactive P1 and P4 sites that contributed to the altered inhibitory activity of choanepins. We constructed a single mutant (choanepin9M T57M) and a double mutant (choanepin9M T57M A60M) of the reactive P1 (A60) and P4 (T57) sites of choanepin9, which were predicted from the alignment (Fig. 1a). These mutant proteins carried altered P1 and P4 sites of choanepin9 to increase the inhibitory activity against subtilisin, mimicking those (M73 for the P1 site and M70 for the P4 site) of bacterial SalSSI containing subtilisin as its cognate protease (Fig. 1a and b). We also mutated the P1 site (Ala60) of choanepin9 to glycine (choanepin9M A60G) in order to determine whether the A60G mutation abolishes the inhibitory activity of choanepin9. Since the P1 site of inactive choanepin8 is glycine, we assumed that the P1 site of choanepin8 interferes with the inhibitory activity against subtilisin. The activity of subtilisin was further inhibited by both choanepin9M T57M and choanepin9M T57M A60M, which had higher inhibitory activity against subtilisin than wild-type choanepin9M (Table 2). The enhanced inhibitory activity coincided with increased affinity. Choanepin9M T57M and choanepin9M T57M A60M showed lower K_d values (2 nM and 12 nM, respectively) than choanepin9M (21 nM) (Table 2). However, the inhibitory activity of choanepin9M A60G was abolished, as expected (Table 2). The higher K_d value of choanepin9M A60G (47 nM) also indicated decreased affinity for subtilisin (Table 2). To test whether the mutations in the P1 and P4 sites affect the substrate specificity of choanepin9, we determined the inhibitory activities of
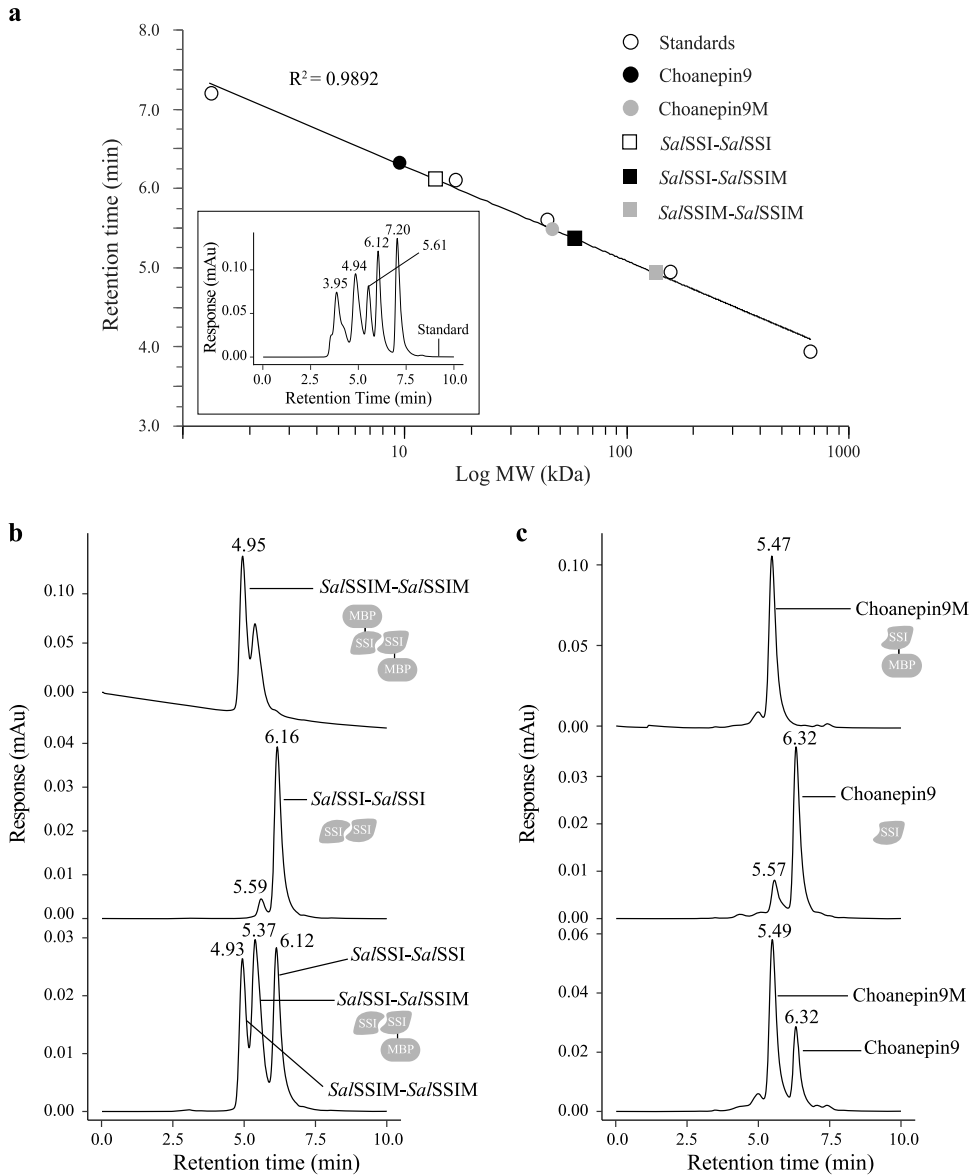
FIG 4 Size exclusion chromatography of choanepin9 and *Sal*SSI. The oligomeric states of *Sal*SSI and choanepin9 were determined by size exclusion chromatography using a Bio SEC-5 300 Å column in a mobile phase containing 20 mM Tris-Cl, 0.3 M NaCl (pH 7.5). (a) Calibration curve plotted with the size exclusion standards to determine the molecular weights of choanepin and *Sal*SSI. (Inset) Elution times of size exclusion standards (670 kDa, 158 kDa, 44 kDa, 17 kDa, and 1.3 kDa). (b) HPLC chromatograms of *Sal*SSI, *Sal*SSIM, and the *Sal*SSI-*Sal*SSIM mixture. Au, absorbance unit. (c) HPLC chromatograms of choanepin9, choanepin9M, and the choanepin9-choanepin9M mixture. In panels b and c, the top and middle portions show homogeneous *Sal*SSI or choanepin9 with and without MBP fusion, respectively, while the bottom portions show the heterogeneous equimolar mixture of MBP-fused and nonfused *Sal*SSI or choanepin9.

choanepin9 T57M and choanepin9 T57M A60M against proteinase K, trypsin, and α-chymotrypsin (Fig. S1). Choanepin9 and choanepin9 T57M showed low inhibitory activity against proteinase K, but choanepin9 T57M A60M showed no inhibition. Choanepin T57M A60M showed a 25% decrease in α-chymotrypsin activity from that for the uninhibited enzyme, but choanepin9 and choanepin9 T57M showed no inhibition. Trypsin was not inhibited by wild-type or mutant choanepin9.

To investigate structural integrity following changes in the affinity and activity of choanepin9 due to the disulfide bond, we mutated Cys58 in choanepin9 to serine (choanepin9M C58S). Even though choanepin9M C58S contained intact reactive P1 and P4 sites, it completely lost subtilisin inhibitory activity, similarly to choanepin9M A60G,
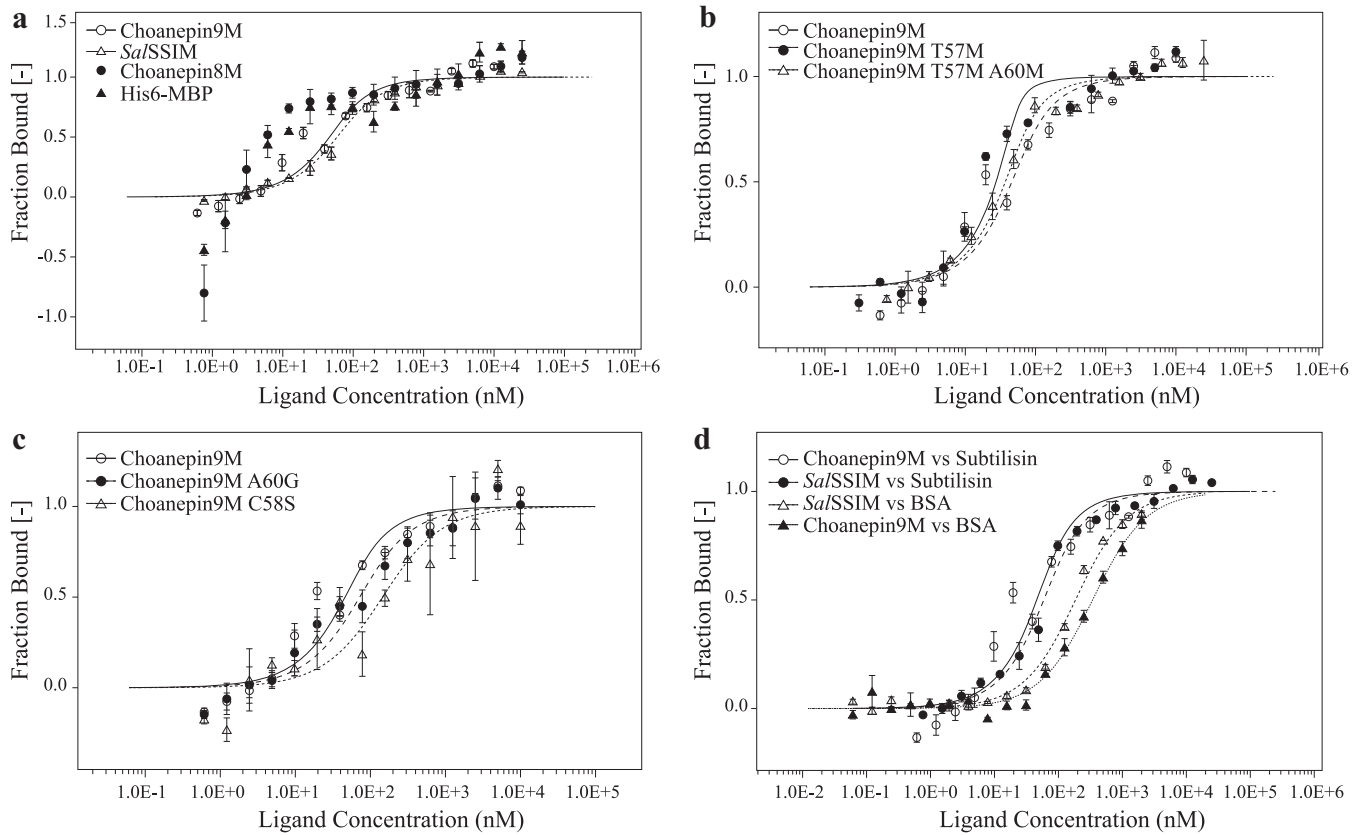
FIG 5 Binding affinities of SSI proteins for subtilisin. Protein-protein interactions between subtilisin and various inhibitors were measured by MST. Dose-response curves for the binding of subtilisin to different inhibitors are shown here. (a) Binding affinities of SalSSIM, choanepin9M, choanepin8M, and MBP-His6 for subtilisin. Choanepin8M and MBP-His6 show nonspecific binding to subtilisin. (b) Binding affinities of choanepin9M, choanepin9M T57M, and choanepin9M T57M A60M for subtilisin. (c) Binding affinities of choanepin9M, choanepin9M C58S, and choanepin9M A60G for subtilisin. (d) Binding of choanepin9M and SalSSIM to subtilisin and BSA. BSA was used to determine the nonspecific binding of choanepin9M and SalSSIM. The K_d values for BSA with choanepin9M and SalSSIM are 943 nM and 294 nM, respectively. These values indicate that choanepin9M and SalSSIM have low affinities for other nonspecific targets. In these experiments, the inhibitor concentration was kept constant at 50 nM, and subtilisin or BSA was titrated in a 16-step serial dilution.

but presented a much higher K_d value (123 nM) than choanepin9M A60G, indicating decreasing binding affinity to subtilisin via structural changes (Table 2).

To determine the effect of structural integrity on reactivity, we mutated Arg90 of bacterial SSI (SalSSI), known as the major contact in the dimer interface (Fig. 1b), to obtain a monomeric form. Arg90 is held tightly in a pocket of the opposite subunit comprising Thr15, Ala22, Pro27, and Leu79 via hydrophobic interactions (19). The Arg90 of SalSSI was mutated to alanine (SalSSIM R90A) in order to determine whether monomeric SalSSI was obtained and remained still active to inhibit subtilisin. We determined the oligomeric state of SalSSIM and SalSSIM R90A by size exclusion chromatography. The molecular weights of native SalSSIM and SalSSIM R90A (the

TABLE 2 Inhibitory activities of choanepin9 mutants against subtilisin[a]

Inhibitor	Residual activity of subtilisin (%)	Specific inhibitory activity (U/mg)	Binding affinity to subtilisin (K_d) (nM)
Choanepin9M	48.7 ± 2.1	0.305 ± 0.028	21
Choanepin9M T57M	9.2 ± 0.8	0.540 ± 0.033	2
Choanepin9M T57M A60M	11.7 ± 1.9	0.523 ± 0.040	12
Choanepin9M A60G	98.9 ± 7.3	0.006 ± 0.001	47
Choanepin9M C58S	98.9 ± 6.4	0.006 ± 0.001	123
SalSSIM	3.4 ± 0.4	0.574 ± 0.030	34
SalSSIM R90A	81.9 ± 4.9	0.108 ± 0.049	132

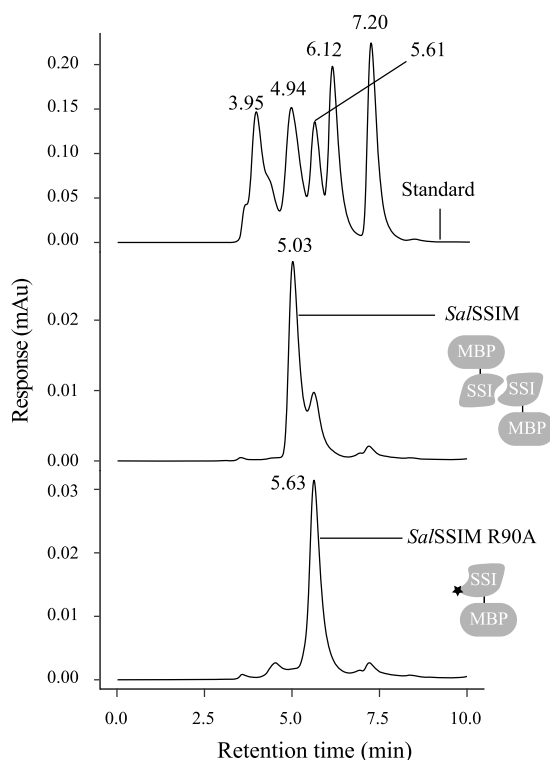[a]Data are presented as means ± standard deviations ($n = 3$).

FIG 6 Size exclusion chromatography of monomeric *Sal*SSIM. The oligomeric state of *Sal*SSI R90A was determined by size exclusion chromatography using a Bio SEC-5 300 Å column in a mobile phase containing 20 mM Tris-Cl, 0.3 M NaCl (pH 7.5). (Top) Elution times of the protein standards (670 kDa, 158 kDa, 44 kDa, 17 kDa, and 1.3 kDa). (Middle and bottom) Homogeneous *Sal*SSIM and *Sal*SSIM R90A, respectively.

theoretical MW of both monomers is 55.2 kDa) were estimated at 112.1 kDa and 36.9 kDa, respectively (Fig. 6), indicating that *Sal*SSIM R90A exists as a monomer. The inhibitory activity of *Sal*SSIM R90A against subtilisin decreased by 81% from that of dimeric *Sal*SSIM (Table 2), although there was no change in reactive sites. We also detected a higher K_d value (132 nM) for *Sal*SSIM R90A than for dimeric *Sal*SSIM (34 nM), suggesting that the affinity of monomeric *Sal*SSIM for subtilisin can be modulated by point mutations reducing structural integrity.

DISCUSSION

The distribution of *Streptomyces* subtilisin inhibitors in bacteria is limited to the phylum *Actinobacteria*. Although several orders within the phylum *Actinobacteria* possess SSI-like proteins, the vast majority belong to the genus *Streptomyces*. A few phytopathogenic or endophytic *Streptomyces* species colonize and invade the host (25). SSI-like proteins have also been found in other endophytic actinobacteria that belong to the genera *Microbispora*, *Nocardia*, and *Micromonospora*. Along with the discovery of fungal SSI-like proteins in plant-pathogenic fungi, these findings emphasize the role of SSI in host-pathogen interactions. SSI-like proteins were found in very narrow taxonomic ranges of fungi and bacteria, but the orthologous relationship was obscure in their gene tree (Fig. 1c). Although the fungal SSI-like genes might emerge via horizontal gene transfer, the origin is not obvious, due to the rarity of SSI-like proteins in the two domains. Sequence analysis showed that fungal SSI-like proteins exhibit their own characteristic features while sharing key structural features with bacterial SSI. Further, this evidence suggests that choanepins may have a yet undiscovered cognate fungal protease, which has key structural differences from subtilisin.

The SSI-like domain inhibits protease activity via noncovalent interaction with the flexible long loop that fits into the substrate-binding pockets of the proteases

(17). We focused on the key amino acid residues contributing to "reactivity" and "structural integrity," which mainly contribute to protease specificity and binding affinity. Amino acid residues and their interactions within the interface region between the enzyme and inhibitor are crucial for reactivity. The reactive P1 and P4 sites are the major determinants of the specificity of *Streptomyces* subtilisin inhibitors (9, 18, 19). Choanepin9M T57M and choanepin9M T57M A60M, which carry mutated P1 (Ala60) and P4 (Thr57) sites, demonstrate the importance of methionine at the P1 and P4 sites, resulting in the inhibition of subtilisin. As shown in the multiple sequence alignment, the presumed P1 site of wild-type choanepin9 is alanine. The P1 site mutation from methionine to alanine (M73A) of *Sal*SSI conferred strong inhibition activity against subtilisin similar to that of wild-type *Sal*SSI (9). We demonstrated that the addition of a second mutation (A60M) to choanepin9 T57M did not change the overall inhibition activity. In contrast, choanepin9M A60G, with glycine at the P1 site, showed a decrease in inhibitory activity due to the absence of interacting side chains, as the *Sal*SSI mutant (M73G) did (9). As a result, the single alteration of the presumed P4 site of choanepin9 to methionine (choanepin9 T57M) was sufficient to enhance inhibitory activity against subtilisin over that of wild-type choanepin9 with alanine at the P1 site. Our findings suggested that the amino acid residues in the presumed P1 and P4 sites of choanepins can be modified to manifest inhibitory activity against subtilisin. From a protein engineering perspective, both presumed P1 and P4 sites are crucial for the modulation of subtilisin inhibitory activity. Thus, presumed P1 and/or P4 sites of choanepin9 represent ideal targets for the design of novel subtilisin inhibitors.

The lack of inhibitory activity of choanepin8 and choanepin3, tested in this study, can be explained by the lack of appropriate P1/P4 sites required for substrate specificity. The activity of serine protease inhibitors is often limited to a narrow range of cognate proteases and does not affect other cellular serine proteases. Human vaspin specifically inhibiting kallikrein 7 protease is one such example illustrating the target specificity of protease inhibitors (26). Thus, we assume that choanepins are also narrow-range protease inhibitors that have specific natural target proteases other than bacterial subtilisin. The partial inhibition of subtilisin by choanepin9 may be an outcome of less-stringent target specificity of the enzyme, which contains a target protease structurally similar to subtilisin. The cognate proteases of choanepins need to be isolated in order to determine the sequence characteristics of their reactive sites.

*Sal*SSI showed similar inhibition activities toward subtilisin and proteinase K. Since subtilisin and proteinase K belong to the same serine protease family, S8, *Sal*SSI might use similar mechanisms to inhibit subtilisin and proteinase K. We observed a low level of proteinase K inhibition by choanepin9 T57M and a low level of α-chymotrypsin inhibition by choanepin9 T57M A60M. These different inhibitory activity profiles toward subtilisin, proteinase K, and α-chymotrypsin could be due to the differences in their subsite structures. The main reactive site and subsites of proteinase K, trypsin, and α-chymotrypsin may not be complementary with choanepin9. However, the P1 and P4 site mutations might have created a low level of complementarity between protease and inhibitor that resulted in a low level of inhibition. In the literature, it was reported that the P1 and P4 site mutants of *Sal*SSI had different inhibitory activity profiles against trypsin, α-chymotrypsin, and lysyl endopeptidase. It was suggested that structural complementarity of the main reactive site and subsites are the important factors that determine substrate specificity (9, 18, 19).

The inhibitory activity of SSI-like proteins is exerted by the noncovalent binding between inhibitor and protease. Thus, the structural integrity that affects binding affinity is another major factor contributing to the activity. The conserved cysteine residues maintain the structural rigidity of the *Streptomyces* subtilisin inhibitor (16, 27). These disulfide bonds are conserved in choanepins to serve the same molecular function (Fig. 1a). The choanepin9 C58S mutant, which lacks the ability to form disulfide bonds but possesses intact reactive sites, failed to inhibit subtilisin and showed decreased affinity to subtilisin. This finding suggests that the four conserved cysteine

residues in all SSI domains except for one choanepin contribute to the inhibitory function of SSI-like domain-containing proteins by maintaining structural integrity.

A major discovery of this study is that choanepin9 acts as a monomer, unlike bacterial SSI, which is a homodimer. We constructed a monomeric bacterial SSI by altering Arg90 of SalSSI, which is held tightly in a pocket of the opposite subunit via hydrophobic interactions (28). The SalSSI R90A mutant was designed as a monomer that lacks the ability to dimerize, and its inhibitory activity against subtilisin was almost abolished. The decreased affinity of SalSSI R90A for subtilisin suggested that monomeric bacterial SSI failed to maintain structural integrity, although the reactive sites were still intact. The subunit-subunit interface of bacterial SSI is formed by β-sheets, in which the β-sheet of one subunit is stacked on a β-sheet of the other subunit. The amino acid sequence within the interface region is highly conserved in bacterial SSI-like proteins (16, 28). However, the corresponding regions of fungal SSI-like proteins are not well conserved. Particularly, the regions corresponding to the first and the second β-strands of bacterial SSI are not conserved in fungal SSI due to frequent insertions and deletions. These observations suggest that the bacterial and fungal SSI evolved divergently at the genome level to maintain their structural integrity in terms of monomeric or dimeric forms.

Conclusion. In this study, we performed molecular and functional characterization of three putative SSI-like domains from the plant-pathogenic fungus *C. cucurbitarum*. Even though they were annotated as SSI-like domains, choanepins showed sequence and molecular features distinct from those of bacterial SSI-like domain-containing proteins. We examined the sequences and functionality of choanepins based on reactivity and structural integrity via site-directed mutagenesis. Our results suggest that choanepins sequentially diverged and duplicated within the fungal genome to target specific cognate proteases and act as monomers. Even though the natural cognate proteases are still unknown, the molecular characteristics of functional choanepin9 elucidated in this study provide a guide to the identification of the target proteases of other choanepins.

MATERIALS AND METHODS

Sequence analysis and structure-guided alignment. The nucleotide and protein sequences of SSI-like domains of *C. cucurbitarum* KUS-F28377 have been reported previously (20). Amino acid sequences of 11 SSI-like domains of *C. cucurbitarum* KUS-F28377, 3 from *A. glauca*, 1 from *A. repens*, and 3 from *B. meristosporus* were retrieved from the UniProt database. These sequences were analyzed with InterProScan 5.25–64.0 (29) to identify SSI-like domains and signal peptides. We truncated the signal peptide regions from the retrieved sequences for multiple sequence alignments, which were performed using the Muscle program (30) (https://www.ebi.ac.uk/Tools/msa/muscle/). A gene tree was constructed using the R package for analysis of phylogenetics and evolution (APE) (31) with the neighbor-joining method, based on 100 bootstrap iterations. The crystal structure of the *Streptomyces* subtilisin inhibitor–subtilisin complex (PDB ID 2SIC) (16) was used to retrieve structural information. The atomic model and sequence alignment were drawn by UCSF Chimera (32).

Molecular cloning and expression of putative fungal SSI-like domains. Three representative genes containing SSI-like domains of *C. cucurbitarum* KUS-F28377 (choanepin8 [UniProt ID A0A1C7N6D3], choanepin9 [UniProt ID A0A1C7N2Q4], and choanepin3 [UniProt ID A0A1C7MXR2]) and SSI from *S. albogriseolus* (UniProt ID P01006.2) were selected for cloning. Selected sequences were codon-optimized for expression in *Escherichia coli* strain B, and gene fragments were chemically synthesized (Integrated DNA Technologies, Coralville, IA, USA) (Table 3). Signal peptide sequences were predicted using InterProScan 5.25–64 with the -appl SignalP option (29) and were removed from the gene fragments for cytosolic expression. Codon-optimized gene fragments were PCR amplified using the primers listed in Table 4. Gene fragments were cloned into a modified pET21a vector (pB3/His6, pB4/MBP-His6, pB6/TRX-His6; provided by the Structural Genomics Center, UC Berkley) (Table 5) via ligation-independent cloning (LIC) (33). N-terminal maltose-binding protein (MBP) and thioredoxin (TRX) tags were added to enhance solubility. A 6-histidine tag was added to facilitate protein purification via immobilized metal affinity chromatography (IMAC). Plasmids were propagated and maintained in *E. coli* DH10B (34) using Luria-Bertani medium (BD Biosciences, San Jose, CA, USA) supplemented with 100 μg/μl of ampicillin (Duchefa Biochemie, Haarlem, Netherlands). The plasmids possessing the SSI-like genes were transformed into *E. coli* BL21(DE3) (35) for protein expression. The cells were grown until mid-log phase at 37°C in LB medium containing 100 μg/μl of ampicillin and were induced by 1 mM isopropyl-β-D-thiogalactopyranoside (IPTG) (Duchefa Biochemie, Haarlem, Netherlands) at 37°C for 4 h in a shaking incubator.

TABLE 3 Sequences of codon-optimized SSI-like gene fragments used in this study

SSI-like gene	Sequence (5′–3′)
Choanepin3	ATGGCGTCAAAGCGGGGGCTTACCAACCTTACTATAACAGCAGAAATTGACATACGGAAGGAAATTCGGTCCCTTCGCTGTAGCCCTACTGGC GGTGACCATCCCCAAAAAGAAGAGGCTTGTCGGCAATTAGGTCGGGCGAATCGGGACCTTAAAGGCCTTCAGGAAACCGACTGTCCGTT CGTCGGAATTCCTGTCACCGTGACAATCGAAGGAAAACTTAGAAACCAACCTGTCTTCTTGACCGAATCCTTTCTGGGGTATTGCGACGC GATCCGTCGCTTTGGCGTAGTTGTTAAAGATGTGTTGCCTAGTTTTTATGAGTAG
Choanepin8	ATGGCCTCCTGTCCCGAGCGTCATACCGTTTTAGCCATTGCGTATCATAACGAAGATCAGGAGATCCGGGCGGATACGTTGGTATGCAATCCA GTGGGGGGGGACCCATCCCAATGCAACGGCGGCATGTGATCTTTTGGAGTCGGTAAATGGTGAGCTTGACGATATTGAGCCGTTGGATCGT TATTGCCGGGGAACCGATTATTTTGCAAATGTCACAATCAAGGGAACATATGAGGGCAAACCCATTGATTTTAAGCACAAATACAGAAAC GGGTGTTATGCGTTAGTGCGGTTGAAGGTGCTTGTCGAGCATTTTCTTGATTACAAGTAG
Choanepin9	ATGTTCAAATCCGCACTTTGTTTAGTTGCCAGTTTTGTTTTGCTGGTCAGCGCGGCACCGGCTACAAACGACGTCCTGACCGTCAGTTCAACCG CTCAAAATGTGAAATACACATTGTCATGCTCGCCTGTCAGCGGGAACCACCCTTATCGCCAGGAGGCCTGTAATGCTCTGAAAAAGTGCGG GGGAAACTTAGACGCGATCACTCCCACTTCGGTAACGTGTCCGGCTCTGTACGCTCCAGTGACCGTGACCATAGAAGGTACATACGGCGG GAAAGCAGTACAACTGAAGAAAGAATATAGCAATGCCTGTACTGCCCAAGCACAGTTAGGGTCTATTGCCCGCCTTTAG
*Sal*SSI	ATGCGTAATACCGGGGCTGGCCCATCCCCCTCAGTAAGCCGTCCACCGCCTTCCGCTGCCCCCCTTTCCGGGGCAGCCTTAGCTGCACCAGGT GATGCGCCTTCTGCTCTGTATGCCCCTAGTGCTCTGGTCTTAACAGTAGGCAAAGGTGTATCGGCTACGACGGCCGCGCCCGAGCGTGCAG TGACACTGACTTGCGCTCCCGGGCCCTCCGGGACTCATCCCGCTGCTGGTTCAGCTTGTGCCGATTTAGCTGCGGTTGGAGGGGATTTGAA CGCTCTTACACGCGGGGAGGATGTGATGTGCCCTATGGTTTACGACCCTGTCTTGTTGACTGTTGACGGGGTTTGGCAAGGTAAGCGTGTT TCCTATGAACGTGTGTTCAGTAACGAGTGTGAAATGAATGCACACGGGTCCTCCGTTTTTGCGTTTTAG

Purification of recombinant proteins. Cells were harvested by centrifugation at $5,000 \times g$ for 20 min at 4°C. Harvested cells were resuspended in a lysis buffer (20 mM Tris-Cl, 100 mM NaCl, 20 mM imidazole, 5 mM beta-mercaptoethanol [pH 7.4]) and disrupted by sonication. The crude cell extracts were centrifuged at $15,400 \times g$ for 20 min at 4°C to separate soluble proteins from cell debris. The resulting supernatant was collected for purification via IMAC with a nickel ion-charged HiTrap HP 5-ml column (GE Healthcare, Chicago, IL, USA) in an LP system (Bio-Rad, Hercules, CA, USA). The column was equilibrated with a 20 mM Tris-Cl–0.3 M NaCl buffer (pH 7.5). The rates of sample loading and elution were set at 3 ml/min and 4 ml/min, respectively. The proteins were eluted by a step gradient of imidazole (0.02 M to 0.5 M) included in the same buffer as the equilibrating buffer. Eluted proteins were analyzed via 10% sodium dodecyl sulfate-polyacrylamide gel electrophoresis (SDS-PAGE), and the target proteins were pooled for further purification via ion-exchange chromatography. The pooled proteins were separated on a HiTrap Q HP 1-ml anion-exchange column (GE Healthcare, Chicago, IL, USA) equilibrated with 20 mM Tris-Cl buffer (pH 7.5) in an LP system. The rates of sample loading and elution were set at 1 ml/min and 2 ml/min, respectively. The recombinant proteins were eluted by a step gradient of salt (0 to 0.5 M) included in the same buffer, and the target fractions were pooled. The collected fractions were concentrated with Amicon Ultra-15 centrifugal filter units (Merck, Germany), with a 30-kDa nominal molecular weight limit, at $3,100 \times g$ for 30 min. The protein concentration was confirmed using a Qubit protein assay kit (Thermo Fisher Scientific, Waltham, MA, USA), and proteins were stored at −80°C in 20% glycerol until further use. We treated the purified proteins with a tobacco etch virus (TEV) protease (New England Biolabs, Ipswich, MA, USA), which cleaves the TEV site of protein to eliminate the MBP tag, if

TABLE 4 Primers used in this study

Primer function and name	Sequence (5′–3′)
Cloning	
Choanepin3_F	GGCGGTGGTGGCGGCATGTTCAAGTTGGTGTTTTTCGC
Choanepin3_R	GTTCTTCTCCTTTGCGCCCCTACTCATAAAAACTAGGCAACAC
Choanepin8_F	GGCGGTGGTGGCGGCATGGCCTCCTGTCCCGAG
Choanepin8_R	GTTCTTCTCCTTTGCGCCCCTACTTGTAATCAAGAAAATGCTCGACAAG
Choanepin9_F	GGCGGTGGTGGCGGCATGGCACCGGCTACAAACGAC
Choanepin9_R	GTTCTTCTCCTTTGCGCCCCTAAAGGCGGGCAATAGACC
SalSSI_F	GGCGGTGGTGGCGGCATGGATGCGCCTTCTGCTCTGTAT
SalSSI_R	GTTCTTCTCCTTTGCGCCCCTACTAAAACGCAAAAACGGAGGACC
Site-directed mutagenesis	
Choanepin9 (T57M)_F	ACAGAGCCGGACACATTACCGAAGTGGGAG
Choanepin9 (T57M)_R	CTCCCACTTCGGTAATGTGTCCGGCTCTGT
Choanepin9 (A60M)_F	GGTCACTGGAGCGTACAGCATCGGACACGTTACCGAAGT
Choanepin9 (A60M)_R	ACTTCGGTAACGTGTCCGATGCTGTACGCTCCAGTGACC
Choanepin9 (T57M A60M)_F	GTACAGCATCGGACACATTACCGAAGTGGGAGTG
Choanepin9 (T57M A60M)_R	CACTCCCACTTCGGTAATGTGTCCGATGCTGTAC
Choanepin9 (A60G)_F	CTGGAGCGTACAGACCCGGACACGTTACC
Choanepin9 (A60G)_R	GGTAACGTGTCCGGGTCTGTACGCTCCAG
Choanepin9 (C58S)_F	GTACAGAGCCGGACTCGTTACCGAAGTGG
Choanepin9 (C58S)_R	CCACTTCGGTAACGAGTCCGGCTCTGTAC
SalSSI (R90A)_F	ACACGTTCATAGGAAACAGCCTTACCTTGCCAAACCCC
SalSSI (R90A)_R	GGGGTTTGGCAAGGTAAGGCTGTTTCCTATGAACGTGT

TABLE 5 Bacterial strains and vectors used in this study

Strain or vector	Description[a]	Reference or source
Strains		
E. coli DH10B	F⁻ endA1 deoR⁺ recA1 galE15 galK16 nupG rpsL Δ(lac)X74 φ80 lacZΔM15 araD139 Δ(ara,leu)7697 mcrA Δ(mrr-hsdRMS-mcrBC) Strʳ λ⁻	34
E. coli BL21(DE3)	F⁻ ompT gal dcm lon hsdS_B(r_B⁻ m_B⁻) λ(DE3 [lacI lacUV5-T7p07 ind1 sam7 nin5]) [malB⁺]_K-12(λ^S)	35
Vectors		
pB3-His6	Modified pET21a vector; a LIC sequence with an N-terminal TEV cleavage site and His tag is inserted.	Structural Genomics Center, UC Berkeley
pB4-MBP-His6	Modified pET21a vector; a LIC sequence with an N-terminal TEV cleavage site, His tag, and maltose-binding protein fusion tag is inserted.	Structural Genomics Center, UC Berkeley
pB6-TRX-His6	Modified pET21a vector; a LIC sequence with an N-terminal TEV cleavage site, His tag, and thioredoxin fusion tag is inserted.	Structural Genomics Center, UC Berkeley

[a]TEV, tobacco etch virus.

necessary. Purified recombinant proteins were stored in a buffer containing 20 mM Tris-Cl, 100 mM NaCl (pH 7.5).

Enzymatic activity assay. The inhibitory activity of SSI was determined based on its potential to inhibit the proteolytic activity of subtilisin. The proteolytic activity of subtilisin was measured using azocasein (both from Sigma-Aldrich, St. Louis, MO, USA) as the substrate. Purified SSI-like proteins and subtilisin were mixed in a 1:2 molar ratio, as described previously (24). Enzyme-inhibitor mixtures were incubated at 37°C for 10 min. After incubation, the substrate was added to start the reaction. The reaction was terminated by adding 400 μl of 5% trichloroacetic acid (TCA) (Sigma-Aldrich, St. Louis, MO, USA) to the reaction mixture. The coagulated protein was removed by centrifugation at 2,200 × g for 5 min, followed by the addition of 150 μl of 0.5 M NaOH to the resulting supernatant for color development. The absorbance was measured at 440 nm. One unit of subtilisin activity was defined as the amount of enzyme that hydrolyzes casein to produce a color equivalent to that produced by 181 μg of tyrosine per min at 37°C (pH 7.5). One unit of inhibitor activity was defined as the reduction of one absorbance unit of TCA-soluble casein in the hydrolysis product released by subtilisin measured at 440 nm per min under the assay conditions (36). Protease inhibitor activity was expressed in terms of residual subtilisin activity. All measurements were carried out in triplicate.

HPLC analysis. The oligomerization states of fungal SSI-like proteins and bacterial SSI were analyzed by high-performance liquid chromatography (HPLC). The samples were analyzed with a Bio SEC-5 size exclusion column (Agilent, Santa Clara, CA, USA). Agilent Bio SEC-5 100-Å and Agilent Bio SEC-5 300-Å columns were used with gel filtration standards (thyroglobulin, gamma globulin, ovalbumin, myoglobin, and vitamin B$_{12}$) (Bio-Rad, Hercules, CA, USA). For the calibration of the Bio SEC-5 100-Å column, an additional protein standard (12.5 kDa) was used with the standards mentioned above. The HPLC system consisted of a 1525 Binary HPLC pump, a 717 Plus autosampler, a 2487 dual λ absorbance detector, and a 2410 refractive index detector (Waters, Milford, MA, USA). The mobile phase buffer contained 20 mM Tris-Cl, 0.3 M NaCl (pH 7.5). The flow rate was set to 0.6 ml/min. The chromatographic data were evaluated and retrieved with Waters Empower2 software (Waters, Milford, MA, USA).

Native gel electrophoresis. The oligomerization of inhibitors was further characterized by native agarose gel electrophoresis, which was conducted with 0.8% agarose (Mbiotech, Republic of Korea) in buffer A (25 mM Tris-HCl, 19.2 mM glycine [pH 7.0]) with the comb in the center of the gel. The agarose gel was submerged in buffer A, and electrophoresis was performed at 50 V for 60 min at room temperature. An equimolar mixture of MBP-fused and nonfused protease inhibitors was compared with a control.

MST assay. The binding affinities of choanepins for subtilisin were determined via microscale thermophoresis (MST) with a Monolith NT.115 instrument (NanoTemper Technologies GmbH, Munich, Germany) (37, 38). Purified His$_6$-tagged proteins were buffer-exchanged with phosphate-buffered saline (PBS; pH 7.5) and quantified using a Qubit protein assay kit (Thermo Fisher Scientific, Waltham, MA, USA). The concentrations of choanepins, bacterial SSI, and MBP with the His$_6$ tag were adjusted to 200 nM before the labeling. His tag labeling was carried out using the RED-tris-NTA 2nd-generation dye according to the manufacturer's guidelines. For affinity determination, subtilisin (Sigma-Aldrich, St. Louis, MO, USA) was dissolved in PBS, followed by a 16-step serial dilution. RED-tris-NTA-labeled, His-tagged proteins were mixed with subtilisin to a final concentration of 50 nM. Samples were incubated for 30 min at room temperature and loaded into MST premium capillaries. Capillaries were loaded into the Monolith NT.115 device, and measurements were obtained at 25°C at 40% light-emitting diode (LED) and 40% MST power. All the measurements were conducted in triplicate and were analyzed using MO.Affinity Analysis software (NanoTemper Technologies GmbH, Munich, Germany). The dissociation constants (K_d) of choanepins and subtilisin were calculated using the saturation binding curve at equilibrium. The fitting function was derived from the law of mass action (39, 40):

$$\frac{[\text{LP}]}{[P_{\text{tot}}]} = \frac{[L_{\text{tot}}] + [P_{\text{tot}}] + K_d - \sqrt{([L_{\text{tot}}] + [P_{\text{tot}}] + K_d)^2 - 4[L_{\text{tot}}] \cdot [P_{\text{tot}}]}}{2[P_{\text{tot}}]}$$

where [LP] is the concentration of the ligand-protein complex, $[P_{\text{tot}}]$ is the concentration of total protein, and $[L_{\text{tot}}]$ is the concentration of total ligand.

SUPPLEMENTAL MATERIAL

Supplemental material is available online only.

SUPPLEMENTAL FILE 1, PDF file, 0.7 MB.

REFERENCES

1. Supuran CT, Scozzafava A, Clare BW. 2002. Bacterial protease inhibitors. Med Res Rev 22:329–372. https://doi.org/10.1002/med.10007.
2. Björck L, Grubb A, Kjellen L. 1990. Cystatin C, a human proteinase inhibitor, blocks replication of herpes simplex virus. J Virol 64:941–943. https://doi.org/10.1128/JVI.64.2.941-943.1990.
3. Habib H, Fazili KM. 2007. Plant protease inhibitors: a defense strategy in plants. Biotechnol Mol Biol Rev 2:68–85.
4. Yang L, Mei Y, Fang Q, Wang J, Yan Z, Song Q, Lin Z, Ye G. 2017. Identification and characterization of serine protease inhibitors in a parasitic wasp. Sci Rep 7:13. https://doi.org/10.1038/s41598-017-16000-5.
5. Law RHP, Zhang Q, McGowan S, Buckle AM, Silverman GA, Wong W, Rosado CJ, Langendorf CG, Pike RN, Bird PI, Whisstock JC. 2006. An overview of the serpin superfamily. Genome Biol 7:216. https://doi.org/10.1186/gb-2006-7-5-216.
6. Hörger AC, Van der Hoorn RA. 2013. The structural basis of specific protease–inhibitor interactions at the plant–pathogen interface. Curr Opin Struct Biol 23:842–850. https://doi.org/10.1016/j.sbi.2013.07.013.
7. Santamaría ME, Diaz-Mendoza M, Diaz I, Martinez M. 2014. Plant protein peptidase inhibitors: an evolutionary overview based on comparative genomics. BMC Genomics 15:812. https://doi.org/10.1186/1471-2164-15-812.
8. Haq SK, Atif SM, Khan RH. 2004. Protein proteinase inhibitor genes in combat against insects, pests, and pathogens: natural and engineered phytoprotection. Arch Biochem Biophys 431:145–159. https://doi.org/10.1016/j.abb.2004.07.022.
9. Kojima S, Nishiyama Y, Kumagai I, Miura K-I. 1991. Inhibition of subtilisin BPN′ by reaction site P1 mutants of Streptomyces subtilisin inhibitor. J Biochem 109:377–382. https://doi.org/10.1093/oxfordjournals.jbchem.a123389.
10. Murao S, Sato S. 1972. S-SI, a new alkaline protease inhibitor from Streptomyces albogriseolus S-3253. Agric Biol Chem 36:160–163. https://doi.org/10.1271/bbb1961.36.160.
11. Terabe M, Kojima S, Taguchi S, Momose H, Miura K-I. 1995. A subtilisin inhibitor produced by Streptomyces bikiniensis possesses a glutamine residue at reactive site P1. J Biochem 117:609–613. https://doi.org/10.1093/oxfordjournals.jbchem.a124752.
12. Taguchi S, Kojima S, Terabe M, Kumazawa Y, Kohriyama H, Suzuki M, Miura K-I, Momose H. 1997. Molecular phylogenetic characterization of Streptomyces protease inhibitor family. J Mol Evol 44:542–551. https://doi.org/10.1007/pl00006178.
13. Oda K, Oyama H, Ito S, Fukiharu M, Miyagawa Y, Takahashi S, Hirose M, Kikuchi N, Nakayama T, Shibano Y. 2001. Cloning and rational mutagenesis of kexstatin I, a potent proteinaceous inhibitor of Kex2 proteinase. Biochem J 355:339–346. https://doi.org/10.1042/bj3550339.
14. Kakinuma A, Sugino H, Moriya N, Isono M. 1978. Plasminostreptin, a protein proteinase inhibitor produced by Streptomyces antifibrinolyticus. I. Isolation and characterization. J Biol Chem 253:1529–1537.
15. Taguchi S, Yamada S, Kojima S, Momose H. 1998. An endogenous target

protease, SAM-P26, of Streptomyces protease inhibitor (SSI): primary structure, enzymatic characterization, and its interaction with SSI. J Biochem 124:804–810. https://doi.org/10.1093/oxfordjournals.jbchem.a022183.
16. Takeuchi Y, Satow Y, Nakamura KT, Mitsui Y. 1991. Refined crystal structure of the complex of subtilisin BPN′ and Streptomyces subtilisin inhibitor at 1.8 Å resolution. J Mol Biol 221:309–325. https://doi.org/10.1016/0022-2836(91)80221-F.
17. Hirono S, Akagawa H, Mitsui Y, Iitaka Y. 1984. Crystal structure at 2.6 Å resolution of the complex of subtilisin BPN′ with Streptomyces subtilisin inhibitor. J Mol Biol 178:389–413. https://doi.org/10.1016/0022-2836(84)90150-5.
18. Kojima S, Kumagai I, Miura K. 1990. Effect on inhibitory activity of mutation at reaction site P4 of the Streptomyces subtilisin inhibitor, SSI. Protein Eng 3:527–530. https://doi.org/10.1093/protein/3.6.527.
19. Kojima S, Obata S, Kumagai I, Miura K-I. 1990. Alteration of the specificity of the Streptomyces subtilisin inhibitor by gene engineering. Biotechnology (NY) 8:449–452. https://doi.org/10.1038/nbt0590-449.
20. Min B, Park J-H, Park H, Shin H-D, Choi I-G. 2017. Genome analysis of a zygomycete fungus Choanephora cucurbitarum elucidates necrotrophic features including bacterial genes related to plant colonization. Sci Rep 7:40432. https://doi.org/10.1038/srep40432.
21. Akwaji PI, Johnson UE, Effiong US, Aniedi-Abasi M, Ntui OE, Johnson UI. 2014. Determination of pathogenicity of Choanephora cucurbitarum (Berkeley and Ravenel) Thaxt, amongst commonly cultivated vegetables in Calabar, Cross River state, Nigeria. Int J Phytopathol 3:55–61. https://doi.org/10.33687/phytopath.003.02.0234.
22. Jashni MK, Mehrabi R, Collemare J, Mesarich CH, De Wit PJ. 2015. The battle in the apoplast: further insights into the roles of proteases and their inhibitors in plant–pathogen interactions. Front Plant Sci 6:584. https://doi.org/10.3389/fpls.2015.00584.
23. Figueiredo A, Monteiro F, Sebastiana M. 2014. Subtilisin-like proteases in plant–pathogen recognition and immune priming: a perspective. Front Plant Sci 5:739. https://doi.org/10.3389/fpls.2014.00739.
24. Inouye K, Tonomura BI, Hiromi K, Sato S, Murao S. 1977. The stoichiometry of inhibition and binding of a protein proteinase inhibitor from Streptomyces (Streptomyces subtilisin inhibitor) against subtilisin BPN′. J Biochem 82:961–967. https://doi.org/10.1093/oxfordjournals.jbchem.a131800.
25. Seipke RF, Kaltenpoth M, Hutchings MI. 2012. Streptomyces as symbionts: an emerging and widespread theme? FEMS Microbiol Rev 36:862–876. https://doi.org/10.1111/j.1574-6976.2011.00313.x.
26. Heiker JT, Klöting N, Kovacs P, Kuettner EB, Sträter N, Schultz S, Kern M, Stumvoll M, Blüher M, Beck-Sickinger AG. 2013. Vaspin inhibits kallikrein 7 by serpin mechanism. Cell Mol Life Sci 70:2569–2583. https://doi.org/10.1007/s00018-013-1258-8.
27. Kojima S, Kumagai I, Miura KI. 1993. Requirement for a disulfide bridge near the reactive site of protease inhibitor SSI (Streptomyces subtilisin

inhibitor) for its inhibitory action. J Mol Biol 230:395–399. https://doi.org/10.1006/jmbi.1993.1157.

28. Mitsui Y, Satow Y, Watanabe Y, Hirono S, Iitaka Y. 1979. Crystal structures of Streptomyces subtilisin inhibitor and its complex with subtilisin BPN′. Nature 277:447–452. https://doi.org/10.1038/277447a0.

29. Jones P, Binns D, Chang H-Y, Fraser M, Li W, McAnulla C, McWilliam H, Maslen J, Mitchell A, Nuka G, Pesseat S, Quinn AF, Sangrador-Vegas A, Scheremetjew M, Yong S-Y, Lopez R, Hunter S. 2014. InterProScan 5: genome-scale protein function classification. Bioinformatics 30: 1236–1240. https://doi.org/10.1093/bioinformatics/btu031.

30. Edgar RC. 2004. MUSCLE: multiple sequence alignment with high accuracy and high throughput. Nucleic Acids Res 32:1792–1797. https://doi.org/10.1093/nar/gkh340.

31. Paradis E, Claude J, Strimmer K. 2004. APE: analyses of phylogenetics and evolution in R language. Bioinformatics 20:289–290. https://doi.org/10.1093/bioinformatics/btg412.

32. Pettersen EF, Goddard TD, Huang CC, Couch GS, Greenblatt DM, Meng EC, Ferrin TE. 2004. UCSF Chimera—a visualization system for exploratory research and analysis. J Comput Chem 25:1605–1612. https://doi.org/10.1002/jcc.20084.

33. Lee J, Kim S-H. 2009. High-throughput T7 LIC vector for introducing C-terminal poly-histidine tags with variable lengths without extra sequences. Protein Expr Purif 63:58–61. https://doi.org/10.1016/j.pep.2008.09.005.

34. Durfee T, Nelson R, Baldwin S, Plunkett G, Burland V, Mau B, Petrosino JF, Qin X, Muzny DM, Ayele M, Gibbs RA, Csörgo B, Pósfai G, Weinstock GM, Blattner FR. 2008. The complete genome sequence of Escherichia coli DH10B: insights into the biology of a laboratory workhorse. J Bacteriol 190:2597–2606. https://doi.org/10.1128/JB.01695-07.

35. Jeong H, Barbe V, Lee CH, Vallenet D, Yu DS, Choi S-H, Couloux A, Lee S-W, Yoon SH, Cattolico L, Hur C-G, Park H-S, Ségurens B, Kim SC, Oh TK, Lenski RE, Studier FW, Daegelen P, Kim JF. 2009. Genome sequences of Escherichia coli B strains REL606 and BL21(DE3). J Mol Biol 394:644–652. https://doi.org/10.1016/j.jmb.2009.09.052.

36. Bijina B, Chellappan S, Krishna JG, Basheer SM, Elyas K, Bahkali AH, Chandrasekaran M. 2011. Protease inhibitor from Moringa oleifera with potential for use as therapeutic drug and as seafood preservative. Saudi J Biol Sci 18:273–281. https://doi.org/10.1016/j.sjbs.2011.04.002.

37. Bartoschik T, Galinec S, Kleusch C, Walkiewicz K, Breitsprecher D, Weigert S, Muller YA, You C, Piehler J, Vercruysse T, Daelemans D, Tschammer N. 2018. Near-native, site-specific and purification-free protein labeling for quantitative protein interaction analysis by MicroScale Thermophoresis. Sci Rep 8:4977. https://doi.org/10.1038/s41598-018-23154-3.

38. Wienken CJ, Baaske P, Rothbauer U, Braun D, Duhr S. 2010. Protein-binding assays in biological liquids using microscale thermophoresis. Nat Commun 1:100. https://doi.org/10.1038/ncomms1093.

39. Swillens S. 1995. Interpretation of binding curves obtained with high receptor concentrations: practical aid for computer analysis. Mol Pharmacol 47:1197–1203.

40. Magnez R, Thiroux B, Taront S, Segaoula Z, Quesnel B, Thuru X. 2017. PD-1/PD-L1 binding studies using microscale thermophoresis. Sci Rep 7:17623. https://doi.org/10.1038/s41598-017-17963-1.